International Journal of Applied Earth Observations and Geoinformation 108 (2022) 102716

Contents lists available at ScienceDirect

International Journal of Applied Earth Observations and Geoinformation

journal homepage: www.elsevier.com/locate/jag

Integrated topographic corrections improve forest mapping using Landsat imagery

He Yin [a,b,*], Bin Tan [c,d], David Frantz [e], Volker C. Radeloff [a]

[a] SILVIS Lab, Department of Forest and Wildlife Ecology, University of Wisconsin-Madison, 1630 Linden Drive, Madison, WI 53706, USA
[b] Department of Geography, Kent State University, 325 S. Lincoln Street, Kent, OH 44242, USA
[c] NASA Goddard Space Flight Center, Greenbelt, MD 20771, United States
[d] Science System and Applications Inc., Lanham, MD 20706, United States
[e] Geography Department, Humboldt-Universität zu Berlin, Unter den Linden 6, 10099 Berlin, Germany

ARTICLE INFO

Keywords:
Atmospheric correction
Illumination condition
Land cover
Model comparison
Time series
Topographic correction

ABSTRACT

In mountainous environments, topography strongly affects the reflectance due to illumination effects and cast shadows, which introduce errors in land cover classifications. However, topographic correction is not routinely implemented in standard data pre-processing chains (e.g., Landsat Analysis Ready Data), and there is a lack of consensus whether topographic correction is necessary, and if so, how to conduct it. Furthermore, methods that correct simultaneously for atmospheric and topographic effects are becoming available, but they have not been compared directly. Our objects were to investigate (1) the effectiveness of two topographic correction approaches that integrate atmospheric and topographic correction, (2) improvements in classification accuracy when analyzing topographically corrected single-date imagery (14 July 2016 and 2 October 2016), versus a full Landsat time series from 2014 to 2016, and 3) improvements in classification accuracy when including additional terrain information (i.e. topographic slope, elevation, and aspect). We developed a physical based model and compared it with an enhanced C-correction, both of which integrate atmospheric and topographic correction. We compared classification accuracies with and without topographic correction using combinations of single-date imagery, image composites and spectral-temporal metrics generated from the full Landsat time series, and additional terrain information in the Caucasus Mountains. We found that both the enhanced C-correction and the physical model performed very well and largely eliminated the correlation (Pearson's correlation coefficient r ranges from 0.06 to 0.24) between surface reflectance and illumination condition, but the physical model performed best (r ranges from 0.05 to 0.11). Both image composites, and spectral-temporal metrics generated from corrected imagery, resulted in significantly ($p \leq 0.05$) higher classification accuracies and better forest classifications, especially for the mixed forests. Adding terrain information reduced classification error significantly, but not as much as topographic correction. In summary, topographic correction remains necessary, even when analyzing a full Landsat time series and including a digital elevation model in the classification. We recommend that topographic correction should be applied when analyzing Landsat satellite imagery in mountainous region for forest cover classification.

1. Introduction

Accurate land cover maps are essential to address critical challenges such as climate change (Pielke, 2005; Pitman et al., 2009), forest fires (Koetz et al., 2008; Langner et al., 2007), urban planning (Martinuzzi et al., 2007; Pauleit and Duhme, 2000), and human disturbances of natural habitats (Hannah et al., 1995; Sanderson et al., 2002). Remote sensing provides a synoptic perspective and periodic view of the Earth's surface and has been widely used for land cover classification. Of the available remote sensing archives, Landsat constitutes the longest consistent archive at a medium resolution (Wulder et al., 2016). After the opening of the Landsat archive in 2008 (Woodcock et al., 2008), a paradigm shift how to utilize Landsat images for land cover classification occurred that includes, for example, national land cover classification, global forest monitoring, imperviousness assessment, and habitat monitoring (Hansen et al., 2013; Wulder et al., 2018). The recent

* Corresponding author at: Department of Geography, Kent State University, 325 S. Lincoln Street, Kent, OH 44242, USA.
E-mail address: hyin3@kent.edu (H. Yin).

https://doi.org/10.1016/j.jag.2022.102716
Received 11 December 2021; Received in revised form 19 January 2022; Accepted 9 February 2022
Available online 17 February 2022
1569-8432/© 2022 The Authors. Published by Elsevier B.V. This is an open access article under the CC BY-NC-ND license (http://creativecommons.org/licenses/by-nc-nd/4.0/).

analysis-ready data (ARD) further helps users to focus on their science instead of data pre-processing (Dwyer et al., 2018), and makes radiometric and geometric corrected Landsat imagery readily available through USGS data distribution centers.

However, topographic correction is seldom implemented in the current Landsat pre-processing tools and there is no topographically corrected Landsat product that is routinely produced and readily available. That is unfortunate because topographic effects lead to changes in observed land surface reflectance for the similar targets in mountainous environments introducing errors in land cover classifications (Vicente-Serrano et al., 2008). In the mountains, the geometry between the sun, the target orientation, and the sensor, can vary from one pixel to another, generates significant changes in the observed spectral characteristics (Tan et al., 2013). For example, the solar radiation incident on a slope varies strongly with slope azimuth relative to the sun. Topographic correction, also known as illumination correction or illumination compensation, aims to minimize the variability of observed reflectance due to topography by correcting for the effects of a variable local incidence angle (Liang, 2005; Richter, 1998).

The lack of topographic correction is partly due to a lack of consensus for which method to implement. There is a plethora of approaches, which have been reviewed elsewhere (Balthazar et al., 2012; Hurni et al., 2019; Sola et al., 2016). From a conceptual and data-processing point of view, there are two main groups of topographic correction methods: stand-alone topographic correction and integrated topographic correction (Table 1A).

The first group of models, the stand-alone correction approaches, do not take atmospheric conditions as the time the image was taken explicitly into account. Popular approaches include band rationing (Ekstrand, 1996), cosine correction (Teillet et al., 1982), Minnaert model (Minnaert, 1941) and C-correction (Meyer et al., 1993; Teillet et al., 1982). The cosine correction is based on the assumption that the surface reflectance on the inclined surface is a function of the ground surface and the incident angle (the angle between a ray incident on a surface and the solar zenith direction). The C-correction improved the cosine correction by adding a C-factor to compensate the diffused irradiance. While the separated correction models are easier to implement, they do not properly account for the interaction between atmosphere and topography, which is a major shortcoming, because atmospheric conditions determine how much of the radiation, is direct versus diffuse, and these two types of radiation require very different topographic correction methods.

The second group of models, integrate atmospheric correction and topographic correction. In the integrated topographic correction atmospheric parameters are estimated, which allows to separate the direct and diffuse solar radiation components, and to model the complex physical interaction between radiation and terrain (Li et al., 2012, 2015; Richter, 1996; Santini and Palombo, 2019; Hill et al., 1995). Recently, openly available toolboxes that integrate topographic with atmospheric correction have emerged, which makes it feasible to correct imagery in a routinely and less costly way (Frantz et al., 2016).

When evaluating the performance of different topographic correction approaches, one question is how spectral reflectance is affected (Hantson and Chuvieco, 2011; Hurni et al., 2019; Pimple et al., 2017; Richter et al., 2009; Vanonckelen et al., 2014), and multiple criteria have been developed to evaluate the accuracy of different correction approaches such as visual check, correlation between spectral reflectance and illumination condition, and land cover reflectance variability (Sola et al., 2016). Another question, and arguably the one that matters most for users (Banskota et al., 2014), is if the topographic correction improves land cover classification, but most of those assessments were limited to a small area (Chance et al., 2016; Dorren et al., 2003; Huang et al., 2008; Moreira and Valeriano, 2014). In the case of forest classification, topographic correction often improves resulting maps (Mikkola and Pellikka, 2002; Phiri et al., 2018; Tan et al., 2013; Vanonckelen et al., 2013; Hill et al., 1995), but not always (Blesius and Weirich, 2005).

Unfortunately, all of studies investigating the influence of topographic correction on land cover classification used only a single image, or a pair of images, and it is unclear if topographic correction is still needed when analyzing a full time series of satellite data. Image composites, such as the day of the year (DOY) provide annual large-area and gap-free surface reflectance data products that greatly improve land cover classification (Griffiths et al., 2013; White et al., 2014). In addition, time series of satellite data can be summarized in spectral-temporal metrics that characterize inner-annual phenological variation, making them valuable for distinguishing different vegetation types, and robust predictors for land cover classifications (Hansen et al., 2014; Yin et al., 2020; Yin et al., 2017). However, existing DOY composite methods do not often include topographic correction in the data processing chain.

Furthermore, terrain information such as elevation, slope and aspect can greatly improve forest classification in mountains (Domaç and Süzen, 2006; Liu et al., 2018), partly because the spatial distribution of land cover is affected by topography (Dorren et al., 2003), but also because slope and aspect provide information about illumination conditions. However, it is unclear whether the terrain data can overcome the need of topographic correction. We examined if topographic correction is still advantageous for forest mapping when such terrain information is already included as input data for classifications.

Our overarching research question was thus whether topographic correction can improve forest mapping using imagery from different seasons and a full Landsat time series for classification. Specifically, we asked the following research questions:

(1) Can topographic effects be reduced using integrated topographic correction approaches?
(2) How do topographic effects affect forest cover classification using single-date imagery and DOY composite and spectral-temporal metrics from Landsat time series?
(3) How much does adding auxiliary terrain information improve forest cover classification?

Table 1
Land cover classes in our classification.

Class	Description
Coniferous forest	Woody vegetation covered by needle-leaved or scale-leaved trees species (>20%) such as Caucasian fir (*Abies nordmanniana*), Caucasian spruce (*Picea orientalis*), and Scots pine (*Pinus sylvestris*)
Broadleaf forest	Woody vegetation covered by flat-leaved tree species (>20%) such as oriental beech (*Fagus orientalis*), sweet chestnut (*Castenea sativa*), and Caucasian elm (*Zelkova carpinifolia*)
Mixed forest	Woody vegetation mixed with coniferous and broadleaf tree species (>20%), neither coniferous nor broadleaf tree species cover > 70% of the canopy
Herbaceous land	Areas covered by herbaceous plants with a tree cover < 20%, including cultivated lands and grasslands.
Water	Open water with < 20% vegetation or soil cover, such as ocean, river, and lakes
Un-vegetated land	Areas with < 20% vegetation cover, covered by bare rock, sand, permanent ice, or building materials

2. Data and method

2.1. Study area

Our study area covers the Western and Central Caucasus, in the border region of Georgia and Russia (Fig. 1). We selected it because of its high diversity in topography (e.g., elevation ranges from 0 to 5642 m above mean sea level, 1506 m on average) and vegetation types, and because of our regional knowledge of the Caucasus mountains. It is located in the transition area from the high Greater Caucasus Mountain ridge to the coastal Colchis Lowland plain of the eastern Black Sea. The

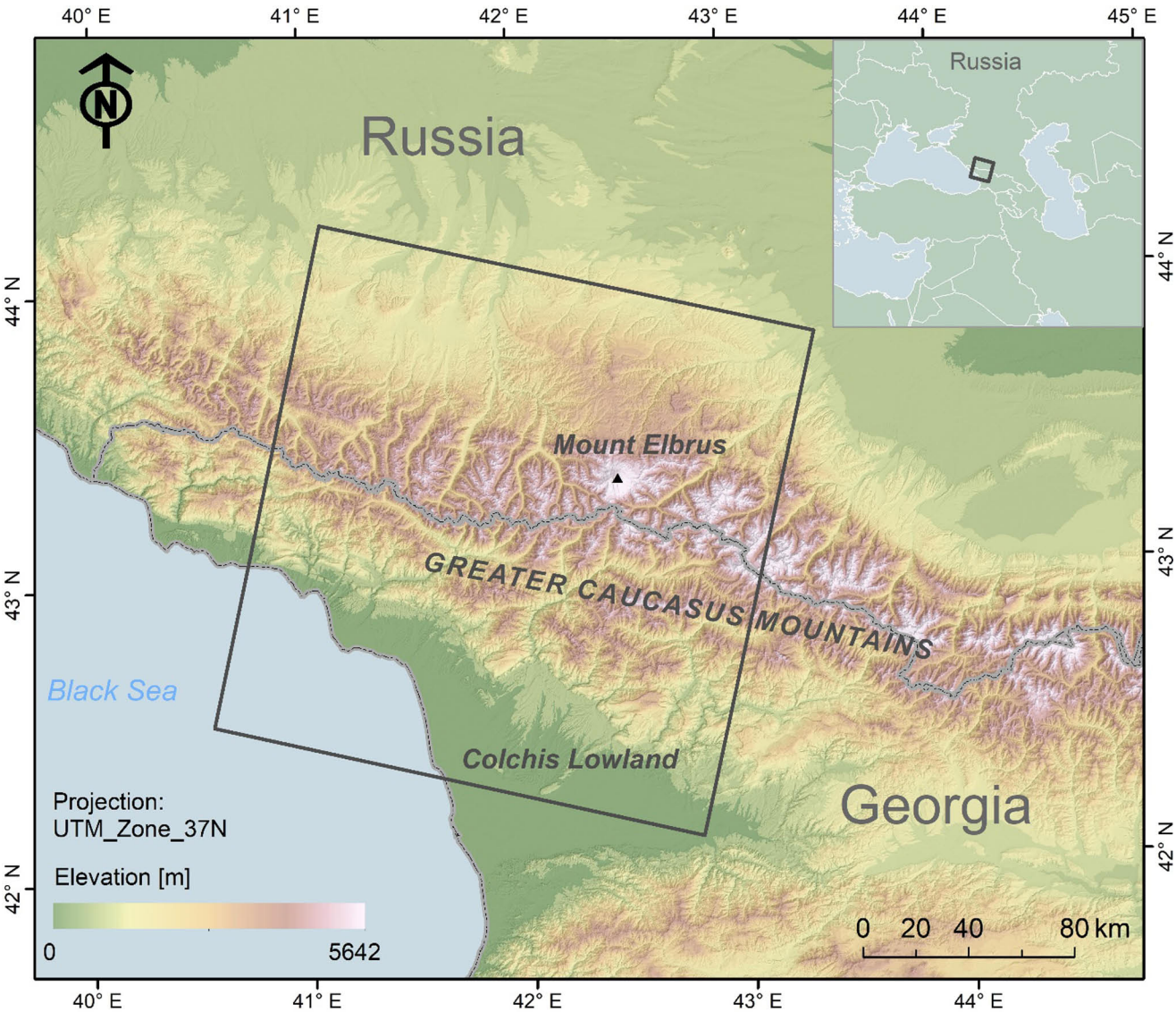

Fig. 1. Topography of the Western and Central Caucasus Mountains. The study area (Landsat path/row: 172/030) is marked as dark gray frame.

Greater Caucasus Mountains have highly variable topography, including Europe's highest mountain (Mount Elbrus), as well as less steep foothills. The length, depth and width of the valleys here vary greatly. In the areas close to the Mount Elbrus, valleys can be 1900 m deep and 7 km wide, and in the Colchis Lowland, valleys are often 1000 m deep and 4 km wide. Our study region has a mean slope of 20 degrees and an elevation of 1506 m (Fig. 1A).

Our study area is situated on the boundary between the temperate and subtropical climatic zone. At lower elevations (<600 m), deciduous trees such as chestnut (*Castanea sativa*), beech (*Fagus orientalis*), oaks (e.g. *Quercus hartwissiana*) and hornbeams (*Carpinus betulus*) dominate the forests. At about 900–1500 m there are wide expanses of beech trees, gradually replaced by a mixed forest of spruce (e.g. *Picea orientalis*), fir (e.g. *Abies nordmanniana*) and beech at higher elevations. From 2,000 m up to the snow line (3,200–3,600 m), mountains are covered by meadow and alpine grasses (Zazanashvili et al., 2000).

2.2. Data and pre-processing2.2.1 Landsat imagery

We analyzed all available Landsat Collection 1 imagery with < 70% cloud cover for the footprint 172/030 from 2014 to 2016 (32 Landsat 7 ETM + and 28 Landsat 8 OLI images). We downloaded the Level 1 digital numbers (DN) product as inputs for our integrated atmospheric and topographic correction (see Section 2.3), and Level 2 surface reflectance as our imagery without topographic correction (see Section 2.4.3), from the United States Geological Survey (USGS, https://earthexplorer.usgs.gov/). To ensure spatial precision, we only used tier 1 imagery.

In additions to our forest mapping based on the entire time series from 2014 to 2016, we analyzed single images obtained on 14 July 2016 (i.e., summer, solar azimuth angle: 134.95; solar zenith angle: 27.59) and 2 October 2016 (i.e., autumn, solar azimuth angle: 158.17; solar zenith angle: 49.25) to examine the performance of our topographic algorithms. We selected these two single-date images because they were the only cloud-free imagery in the summer and autumn of 2016, and because they represented very different illumination conditions (Fig. 2A) and stages of phenology, which was ideal to test how our topographic correction algorithms performed.

2.2.1. Other data

We acquired 1-arc-second (~30 m) Shuttle Radar Topography Mission (SRTM) digital elevation data (DEM) to correct the optical depths, and topographic effect (see Section 2.3) and to compare the influence of terrain information on classification (see Section 2.4.3). The SRTM DEM has an absolute geolocation error of 8.8 m and a height error

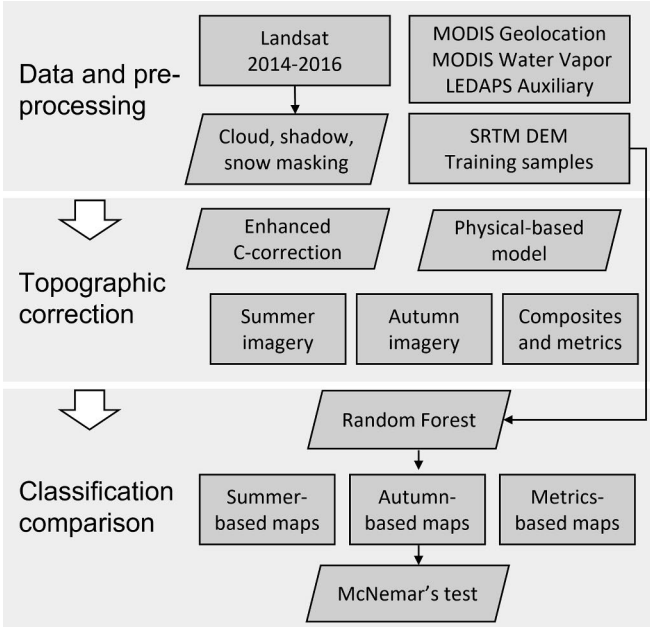

Fig. 2. Data processing workflow.

of 6.2 m at the 90% confidence level in Eurasia (Farr et al., 2007).

To correct water vapor absorption in the Earth's atmosphere, we used the MODIS MOD05, MYD05 products, as well as the MOD03 and MYD03 geolocation tables downloaded from the Level 1 and Atmosphere Archive and Distribution System (LAADS) at NASA's Goddard Space Flight Center (Frantz and Stellmes, 2018; Gao, 2015). We downloaded auxiliary data, such as air pressure, air temperature, and ozone data from USGS website (https://edclpdsftp.cr.usgs.gov/downloads/auxiliaries/ledaps_auxiliary).

2.2.2. Atmospheric correction

The topographic correction methods that we used are both integrated with atmospheric corrections, but differently so. The enhanced C-correction is part of the Framework for Operational Radiometric Correction for Environmental monitoring (FORCE, Frantz, 2019; Frantz et al., 2016). The performance of the FORCE atmospheric correction has been evaluated and compared to other approaches (e.g., LaSRC) in the Atmospheric Correction Intercomparison eXercise (ACIX Doxani et al., 2018). The physical model used 6S radiative transfer code (Vermote et al., 1997) for atmospheric correction (see Section 2.3).

2.3. Topographic correction

We tested two topographic correction methods including an enhanced C-correction model and a physical model (Fig. 2) We selected these two models because they separate the direct and diffuse solar radiation components and model the complex physical interaction between radiation and terrain. Also, the reliability of the enhanced C-correction model used in this study has been demonstrated by previous studies (e.g., Buchner et al., 2020). Both are based on the relative solar incidence angle, or illumination condition (cos i), which we computed following Civco (1989):

$$\cos i = \cos\theta_s \cos\theta_n + \sin\theta_s \sin\theta_n \cos(\phi_n - \phi_s) \quad (1)$$

where i is the angle between solar incident angle and the local surface normal. θ_s is the solar zenith angle. θ_n and ϕ_n are topographic slope and aspect (0 = north), respectively. ϕ_s is the solar azimuth angle. The illumination angle varies between −1 and 1 (maximum illumination).

The first approach that we used for topographic correction was based on a modified C-correction (Kobayashi and Sanga-Ngoie, 2008) as described in Frantz et al. (2016) and Buchner et al. (2020). We used an upgraded version of this correction, which is implemented in the freely available software FORCE v1.1 (http://force.feut.de; Frantz et al., 2016). This approach accounts for both the atmospheric and the topographic effects simultaneously. Key steps include: (1) estimation of the shortwave infrared C-factor for each pixel based on a focal linear regression between cos i and Top of the Atmosphere (TOA) SWIR2 reflectance of pixels similar to the central pixel to account for variations in directional reflectance characteristics; (2) computation of a simplified sky view factor based on terrain slope; (3) image-based estimation of aerosol optical depth over water and dark dense vegetation, and computation of dependent atmospheric variables (Tanre et al., 1979); (4) separation of the irradiance into direct and diffuse terms (Hill et al., 1995; Kobayashi and Sanga-Ngoie, 2008); and (5) propagation of the C-factor through the spectrum based on the ratio of the direct and diffuse irradiance using the general radiative theory provided by Kobayashi and Sanga-Ngoie (2008). The implemented topographic correction in FORCE is not designed to correct areas that receive little illumination. Thus areas with illumination condition ($i \geq 80$ degree) were not expected to be corrected reliably (overcorrection does occur), and areas with self-shadow ($i = 90$ degree) were not corrected at all. These areas are flagged accordingly in the per-pixel quality file that is generated by FORCE. The reader is referred to Buchner et al. (2020) for an in-depth description of this algorithm.

The second model is the physical model-based correction (hereafter: physical model, Hill et al., 1995; Richter, 1996). First we separated the irradiance into direct irradiance and diffuse components based on the parameters retrieved by the 6S atmospheric correction (e.g., Fig. 4A) (Vermote et al., 1997). The slope facing the sun receives both direct and diffuse solar radiation, while the side facing away from the sun receives only the diffuse component (Pellikka, 1996). The anisotropy index, proposed by Hay and Mckay (1985), is then calculated from the partition of the direct irradiance and diffuse components:

$$k = E_{g,dir}/E_0 \quad (2)$$

where k is the anisotropy index, $E_{g,dir}$ is the direct irradiance on the ground, and E_0 is the exoatmospherical solar irradiance.

Second, we separated the diffuse irradiance into circumsolar diffuse irradiance and isotropic diffuse irradiance using the anisotropy index. At last, we used cosine correction for the direct irradiance and the circumsolar diffuse irradiance, and corrected the isotropic diffuse irradiance with the ratio of sky view.

$$E_{g,corrected} = (E_{g,dir} + k^* E_{g,diff})^* \frac{\cos(i)}{\cos(\theta_s)} + (1-k)^* E_{g,diff}{}^* F_{skyview} \quad (3)$$

where $E_{g,corrected}$ is the corrected irradiance on the ground; $E_{g,diff}$ is the diffuse irradiance on the ground; $F_{skyview}$ is the ratio of the sky view. We calculated the ratio of sky view from DEM with a ray tracing approach that averaged 30 partial hemispheres. We coded the physical model for the purpose of this study. When there is no direct irradiance, e.g. the sun is hidden by the topographic features, the pixel is marked and the irradiance is not corrected. Please note that such pixels are rare in the study area.

2.4. Forest classification

2.4.1. Classification scheme

We mapped three forest types: coniferous forest, broadleaf forest, and mixed forest (Table 1). In addition, we mapped herbaceous land, water, and un-vegetated land.

2.4.2. Training data collection

We used Landsat pixels as the unit of our training data. First, we selected 2000 Landsat pixels across our study area using a random sampling design. Stratified sampling can help collecting samples for

classes that cover a small area, but we lack an appropriate land cover map that includes all our mapping classes for stratification. Furthermore, we preferred a random sampling because we wanted to ensure that each sample from the entire population had an equal chance of being selected. Also, a random sampling approach enabled us to investigate how mapping accuracy varied across different illumination conditions. We determined this sample size to ensure high power for our statistical tests of differences in the accuracy of the classifications based on corrected and uncorrected satellite imagery, and the fact that we did find highly significant differences (see Results) confirmed that the sample size was sufficient. Second, we created 3 × 3 m grids covering each training sample (30 × 30 m) and overlaid the grids on high resolution imagery available on Google Earth™ and Bing Aerial™. We selected high-resolution imagery as close as possible to the date of Landsat imagery, and forests changed little in the Caucasus in the past decades (Bragina et al., 2015), so we assumed that land cover change between the dates of our reference data and the satellite data did not affect our accuracy assessment greatly. To ensure the geometric accuracy of the high resolution imagery, we discarded samples that showed inconsistent geolocation (>half-pixel difference) through visual interpretation. We then added the same amount of randomly distributed samples that were geometrically consistency to retain a sample size of 2000. Third, we estimated the area proportion of each land cover class within each sample (30 × 30 m) and assigned the class label based on the majority rule. In order to distinguish different forest types, we used multi-temporal imagery, especially winter imagery, to label the samples. We selected imagery as close as possible to the period 2014–2016. If there was no high resolution imagery available during 2014–2016, we chose the imagery that was closest in date. In case of missing high resolution imagery, we used Landsat imagery instead. In total, we collected 103 coniferous forest samples, 527 broadleaf forest samples, 145 mixed forest samples, 807 herbaceous samples, 195 water samples, and 223 unvegetated land samples.

Though we tried our best to label these samples accurately, some errors may exist. Nevertheless, we applied the same samples to all the imagery for model classification and validation, and for both topographic correction methods, so that the potential errors in our samples did not affect the comparison of mapping accuracy.

2.4.3. Input variables and classification model

We evaluated the performance of our topographic corrections based on three test cases: (1) summer imagery, (2) autumn imagery and (3) DOY composite and spectral-temporal metrics. Within each case, we used six different input datasets for our classification (Table 2): (1) uncorrected imagery (i.e., Level 2 surface reflectance without topographic correction), (2) uncorrected imagery plus terrain information (i.e., topographic slope, elevation, and aspect), (3) corrected imagery using enhanced C-correction, (4) corrected imagery using enhanced C-correction plus terrain information, (5) corrected imagery using physical model, and (6) corrected imagery using physical model plus terrain information. We included summer and autumn imagery to investigate the necessity of topographic correction in different seasons and vegetation growing stages. We selected nearly cloud-free (<1%) Landsat 8 OLI images for July, 14th 2016 and October, 2nd 2016 to represent summer and autumn illumination conditions, respectively. We generated cloud-free image composites by selecting Landsat pixels based on temporal distance to August 1st and percent cloud and spatial distance to next shadow cover (White et al., 2014). We calculated spectral-temporal metrics from all available Landsat imagery because they provide gap-free imagery across large areas and valuable seasonal information for land cover differentiation. We calculated five spectral-temporal metrics: the mean, median, 25% quantile, 75% quantile, and standard deviation for each spectral band from 2014 to 2016. Cloud, shadow, and snow were masked out prior to calculation using the quality band accompanied with Landsat Collection 1 product. Because FORCE is not intended to correct low illuminated areas, we extracted the low illuminated areas

Table 2
18 Sets of input variables used for forests and land cover classification.

Set no.	Group	Classification model inputs
1	Summer imagery	Uncorrected summer imagery
2		Uncorrected summer imagery + Terrain
3		Corrected summer imagery using enhanced C-correction
4		Corrected summer imagery using enhanced C-correction + Terrain
5		Corrected summer imagery using physical model
6		Corrected summer imagery using physical model + Terrain
7	Autumn imagery	Uncorrected autumn imagery
8		Uncorrected autumn imagery + Terrain
9		Corrected autumn imagery using enhanced C-correction
10		Corrected autumn imagery using enhanced C-correction + Terrain
11		Corrected autumn imagery using physical model
12		Corrected autumn imagery using physical model + Terrain
13	Composite and Spectral-temporal metrics	Uncorrected composite and spectral-temporal metrics
14		Uncorrected composite and spectral-temporal metrics + Terrain
15		Corrected composite and spectral-temporal metrics using enhanced C-correction
16		Corrected composite and spectral-temporal metrics using enhanced C-correction + Terrain
17		Corrected composite and spectral-temporal metrics using physical model
18		Corrected composite and spectral-temporal metrics using physical model + Terrain

($i \geq 80$ degree) for each image as additional QA mask. We then compared the classification accuracies with and without applying the QA masks (See section 2.5.1). We also compared classification with and without the normalized difference vegetation index (NDVI). The results showed that NDVI improved accuracy very little, and even decreased mapping accuracy for some classes (Fig. 3A). We therefore decided not to include NDVI in our study.

We used a random forest classifier to map forests and other land cover classes for each set of input images (Belgiu and Drăguţ, 2016). Two parameters, the number of decision trees (*ntree*) and the number of variables randomly sampled as candidates at each split (*mtry*) when growing the trees need to be optimized for building a robust model. First, we tested classification performance for *ntree* ranging from 10 to 1000 and we found that a number of 500 tree was sufficient for a reliable classification (results not shown). Second, we tested *mtry* from two up to the number of input variables at a step of one in each model, and selected the *mtry* value that resulted in the highest classification accuracy for the final model.

2.5. Classification comparison

We used several measures to validate and compare the performance of our classifications, including user's and producer's accuracy, F-measure and McNemar's test.

2.5.1. Accuracy assessment

We derived a confusion matrix from a 5-fold cross validation of the random forest model. The 5-fold cross validation randomly splits the data into five folds of roughly equal size (in our case there are 400 samples in each fold). Each of the folds is left out in turn and the other four folds are used to train the model. The held-out fold is then predicted, and all the predictions are summarized. We repeated the 5-fold cross validation 100 times and summed up the predictions. After the

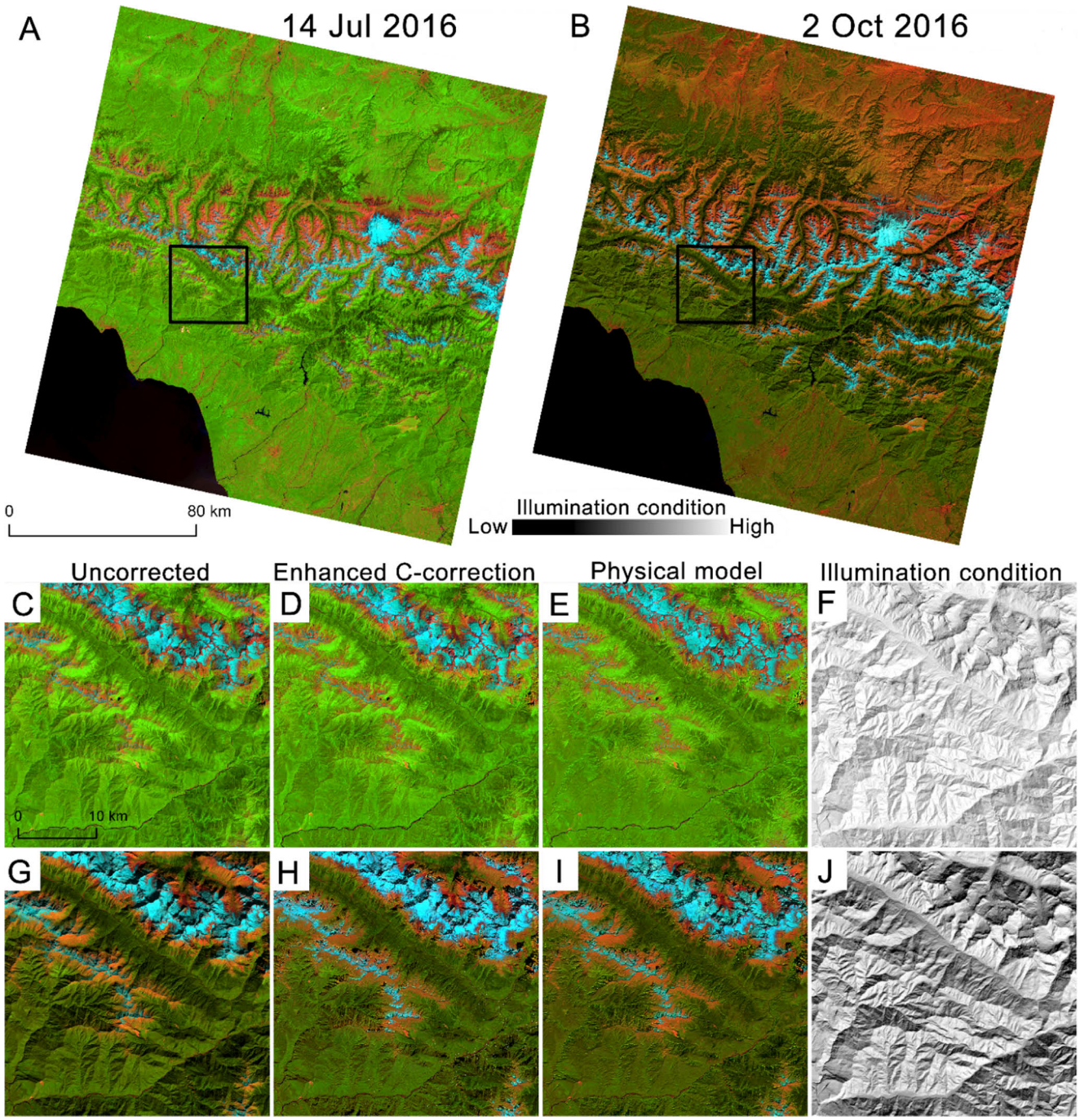

Fig. 3. Landsat summer (panel A) and autumn (Panel B) images (RGB: 743) for the study area. Subset region marked in black frame. Panels C-F show uncorrected (panel C), corrected summer image using the enhanced C-correction (panel D) or the physical model (panel E), and the corresponding illumination condition (F). Panels G-J show the same as panel C-F, but for the autumn image. The QA layers generated from FORCE were not applied here.

validation of the model accuracy, we used all the samples to train the models and calculated user's and producer's accuracy and F-measure from the confusion matrix with and without applying FORCE QA masks. The F-measure, a harmonic mean of user's and producer's accuracy, is advantageous when learning from imbalanced data (Powers, 2011). In addition, we performed an accuracy assessment among different illumination conditions by dividing the illumination condition (IC) for summer imagery into four categories: low illumination (IC < 0.7), low to moderate illumination ($0.7 \leq$ IC < 0.8), moderate to high illumination ($0.8 \leq$ IC ≤ 0.9) and high illumination (IC > 0.9). Similar categories were generated for autumn imagery but with different thresholds: low illumination (IC < 0.5), low and moderate illumination ($0.5 \leq$ IC < 0.6), moderate and high illumination ($0.6 \leq$ IC ≤ 0.7) and high illumination (IC > 0.7).

2.5.2. McNemar's test

To test whether the classifications differed significantly from each other, we applied McNemar's tests. The McNemar's test is a variant of χ^2 test with one degree of freedom under the null hypothesis (Agrest, 1990)

$$\chi^2 = \frac{(n_{21} - n_{12})^2}{n_{21} + n_{12}} \tag{4}$$

Where n_{12} denotes the number of instances in which classification A failed and classification B succeeded. When $\chi^2 = 0$, the two

classifications have similar performance. As χ^2 diverges from 0, their performance differs significantly. The χ^2 can be translated into confidence intervals for one-tailed and two-tailed predictions. We calculated the significance interval (p) of McNemar's test using a paired-classification comparison for three forest types.

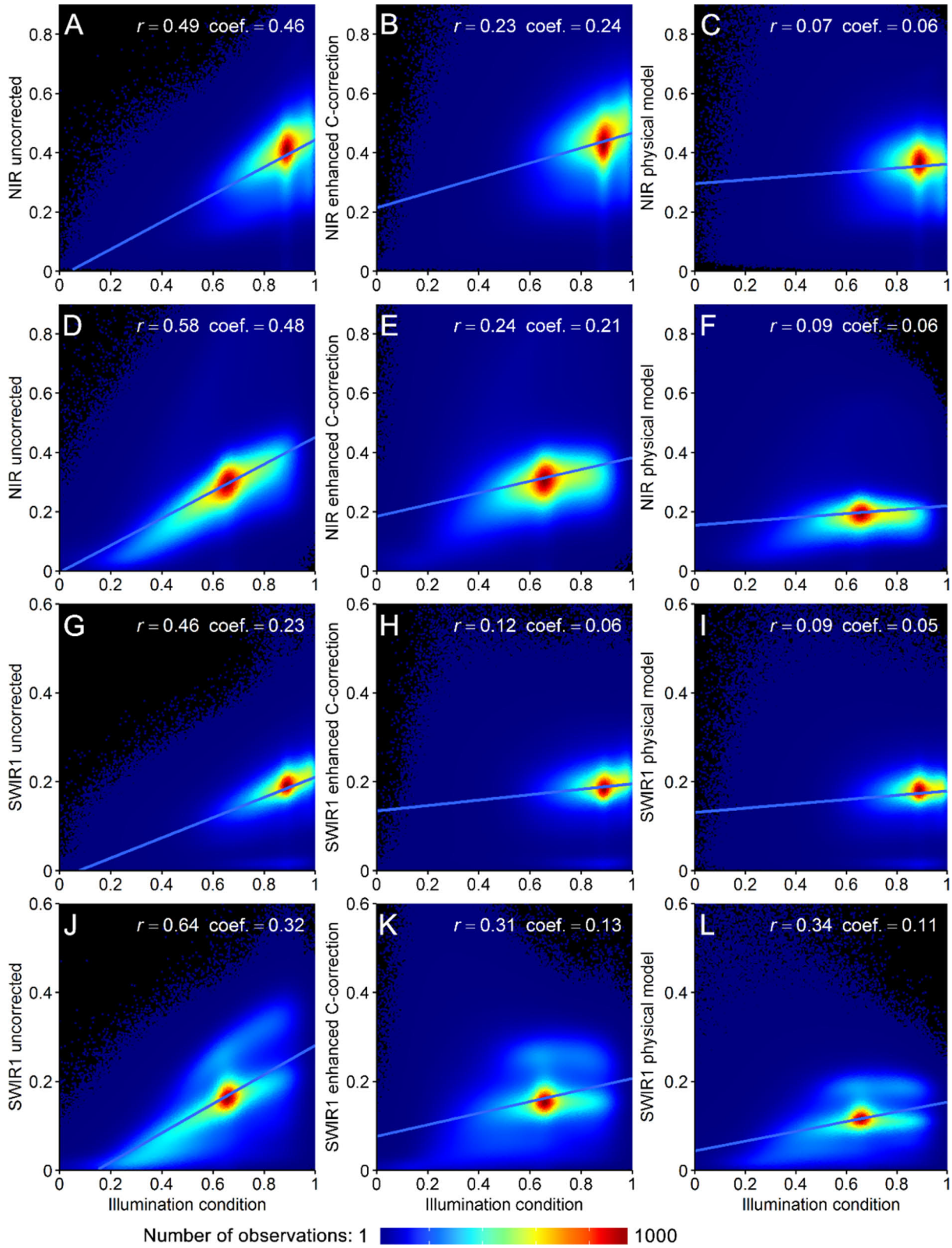

Fig. 4. Landsat NIR and SWIR1 band as a function of illumination condition in summer (panels A-C, G-I) and autumn (panels D-F, J-L). Note that the Black Sea area was masked out.

3. Results

3.1. Topographic correction on Landsat imagery

Visually, both the enhanced C-correction and the physical model greatly reduced variability in reflectance due to topography (Fig. 3). Accordingly, the uncorrected imagery had a clear relationship between illumination condition and spectral reflectance (Fig. 4), for example, in summer NIR (Pearson's correlation $r = 0.49$, coefficient = 0.46) and SWIR1 reflectance ($r = 0.46$, coefficient = 0.23). In autumn, the relationship for SWIR1 was stronger because of lower sun elevation (e.g., $r = 0.64$, coefficient = 0.32). The corrected imagery had a much lower correlations between illumination conditions and the reflectance, ranging from 0.06 to 0.24 for the enhanced C-correction corrected imagery, and 0.05 to 0.11 for the physical model.

3.2. Forest cover classification

3.2.1. Spatial pattern of forests

The classifications of our 18 different sets of input variables resulted in similar patterns of forests (Fig. 5). However, the differences were obvious in areas at the ends of the full range of illumination conditions (Fig. 6). First, in areas with lower illumination conditions, the uncorrected imagery tended to predict more coniferous and mixed forests (Fig. 6, subset A summer imagery). In valleys that received very little direct and diffused irradiation (Fig. 6, subset B autumn imagery), forests were even mapped as water. The uncorrected autumn imagery resulted in even more coniferous forest than the uncorrected summer imagery. Second, topographically corrected imagery generated more consistent classifications across different input variables than the uncorrected imagery, especially when we used the physical based model. Third, we found more consistent classification based on the composite and spectral-temporal metrics compared to single-date imagery. Fourth, the

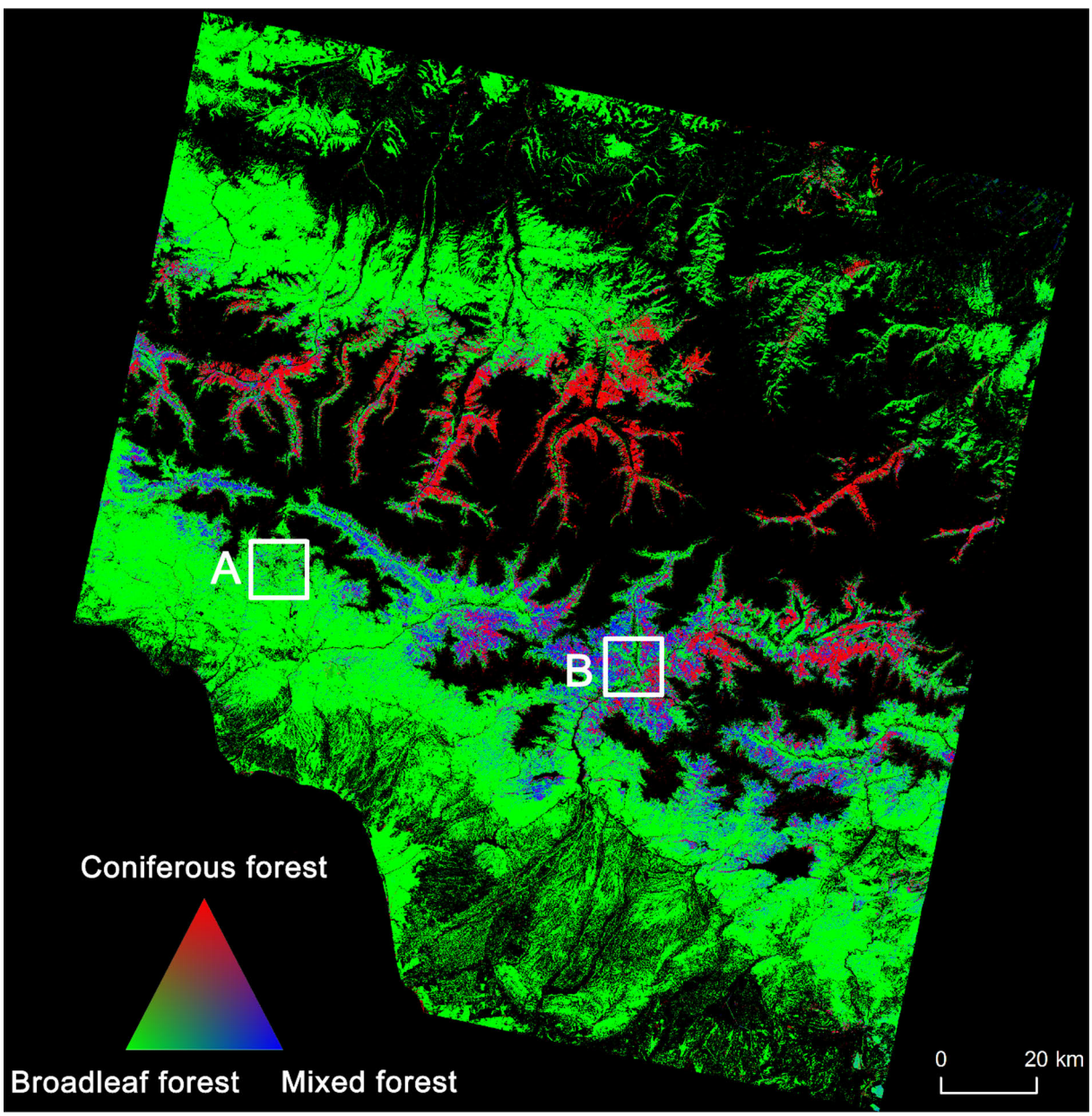

Fig. 5. Forest cover classification agreement among the 18 sets of input variables. Pixels in red color were classified by all sets of input variables as coniferous, in green color as broadleaf forest, and in blue color as mixed forest. Black color indicates that no forest was predicted by any set of input variables. Two subsets A and B which are marked in white frames were zoomed in for a detailed map comparison in Fig. 5.

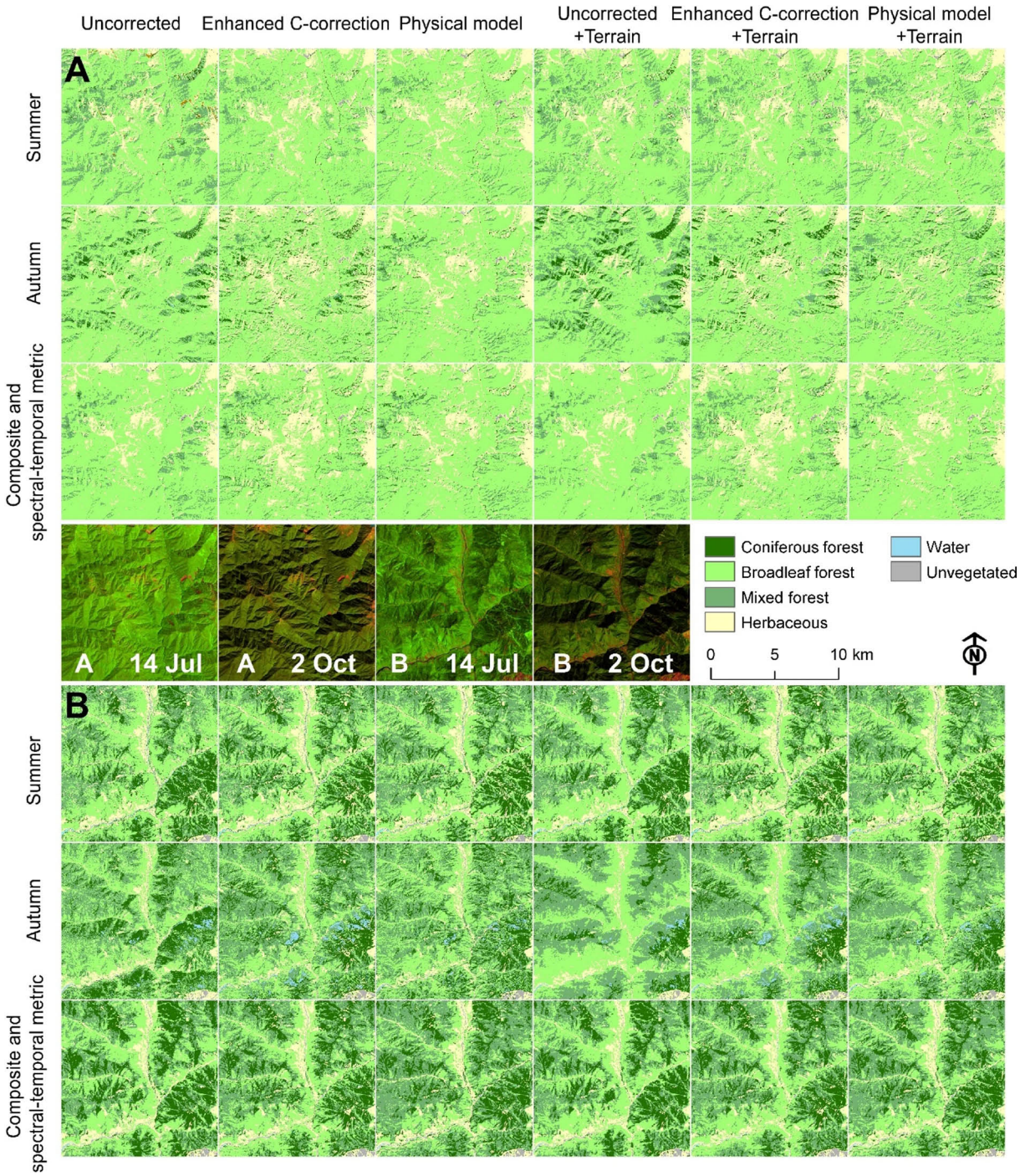

Fig. 6. Forest classification comparison using 18 sets of input variables for subset A (top panel) and B (bottom panel) marked in Fig. 5. The middle panel shows the uncorrected summer (14 July 2016) and autumn (2 October 2016) images (RGB: 743) for these two subsets. Note that the QA layers generated from FORCE were not applied here.

differences in forest pattern were largest where the three forest types intermingled (Fig. 6, subset B).

3.2.2. Forests classification accuracy

Using topographically corrected imagery resulted consistently in higher forest classification accuracies (Fig. 7). The average F-measure of all forest types using topographic corrected imagery was 0.75 and 0.78 for the enhanced C-correction and physical model respectively, compared to 0.70 based on uncorrected imagery. The advantage of topographic correction was strongest when we classified autumn imagery: the F-measure increased 18% and 22% for the enhanced C-correction and physical model corrected imagery, respectively. Classification accuracy also increased when we used composite and spectral-temporal metrics for classification. The F measure increased 3% for the enhanced C-correction and 6% for the physical model corrected imagery.

The biggest improvement of using topographic corrected imagery occurred for the mixed forest class (Fig. 7). Compared to coniferous and broadleaf forest, the mixed forest class was least accurately mapped. The F-measures (without applying the FORCE QA mask) of all sets of input variables for mixed forest ranged from 0.38 to 0.70, while broadleaf forest had F-measures between 0.78 and 0.90, and coniferous forest's

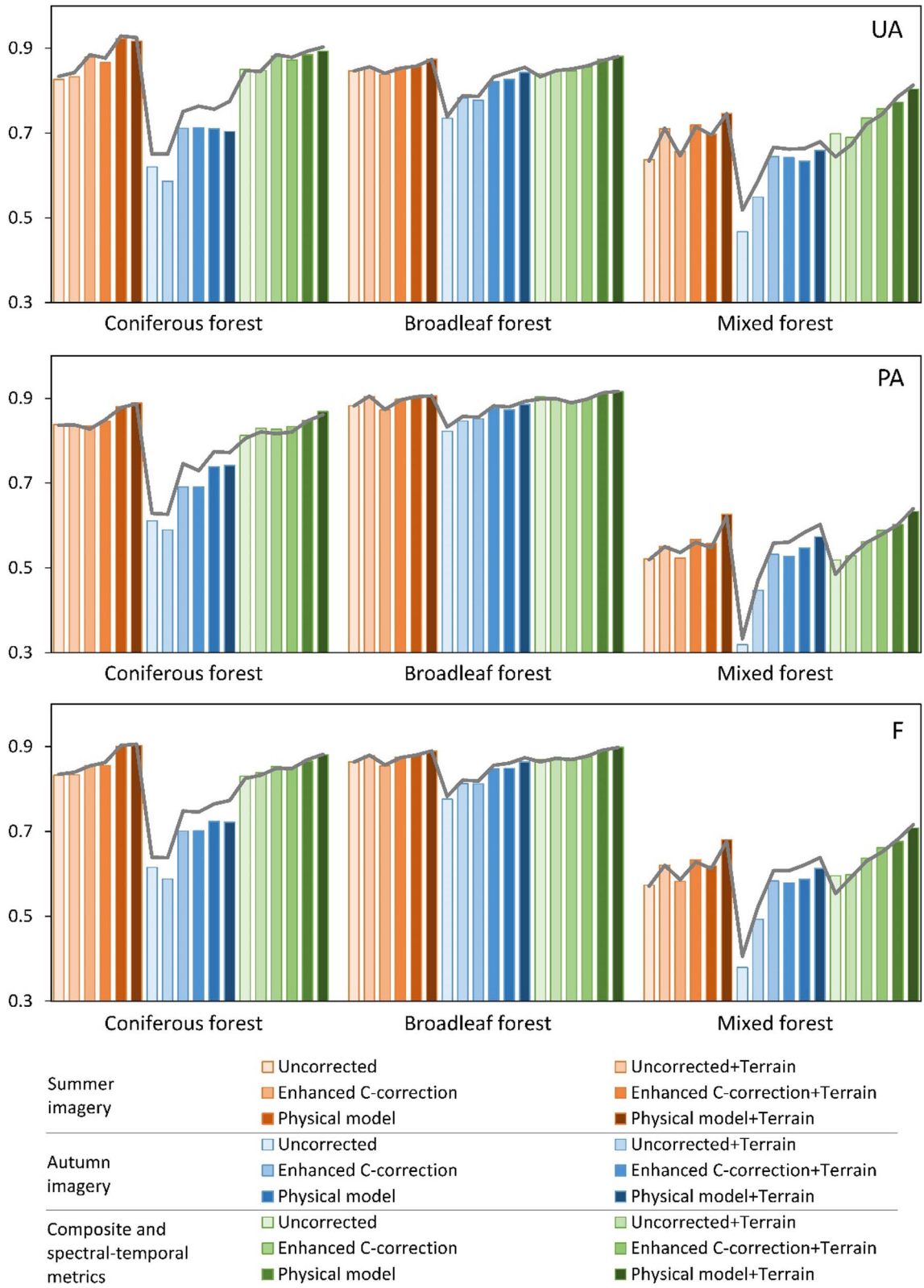

Fig. 7. User's accuracy (UA), producer's accuracy (PA) and F-measure (F) of coniferous, broadleaf and mixed forests for 18 sets of input variables. The bars indicate the accuracies without applying the FORCE QA mask, while the gray lines indicate the accuracies for the areas outside that mask.

between 0.59 and 0.90. However, topographic correction improved mixed forest classification accuracy greatly. The classification accuracy for mixed forest was 0.58 and 0.59 when we classified the enhanced C-correction and physical model corrected autumn image respectively, comparing to 0.38 for uncorrected autumn image. The DOY composite and spectral-temporal metrics derived from physical model corrected imagery yielded the highest mixed forest classification accuracy (0.68).

Including terrain information improved classifications. The average

F-measure was the highest for physical model corrected imagery plus terrain information (0.79), followed by physical model corrected imagery (0.78), enhanced C-correction corrected imagery plus terrain information (0.76), enhanced C-correction corrected imagery (0.75), uncorrected imagery plus terrain information (0.70), and uncorrected imagery (0.70).

Based on the McNemar's tests, differences in classification accuracy using uncorrected and topographic corrected imagery were significant ($p \leq 0.05$) for most sets of input variables except the ones for broadleaf forest classification using summer imagery ($p > 0.05$, Fig. 8). The accuracy of classification improved significantly ($p \leq 0.05$) when we used terrain information. However, for the classification based on physical model corrected imagery, about 44% of classifications resulted in significant ($p \leq 0.05$) improvement when we included terrain information. Similarly, about 78% of classifications that used uncorrected or enhanced C-correction imagery resulted in significant ($p \leq 0.05$) improvement when we used terrain information.

The classification accuracy was generally lower in areas with extreme, e.g., very low or very high, illumination conditions (Fig. 9). For instance, mixed forest had an F-measure of > 0.4 in the areas with moderate illumination conditions ($0.5 \leq IC \leq 0.7$), while in low ($IC < 0.5$) and high ($IC > 0.7$) illumination regions the F-measure dropped to < 0.35 for the uncorrected autumn imagery.

The improvement in classification accuracy using corrected imagery varied according to illumination conditions (Fig. 10). We found the biggest classification accuracy improvement (average increase of $F = 0.08$) using corrected summer imagery in low illumination areas. However, the biggest improvement (average increase of $F = 0.18$) using corrected autumn imagery occurred in areas with high illumination conditions ($IC > 0.7$). For coniferous forest, the biggest classification improvement was in low illumination areas when classifying the corrected summer image (average increase of $F = 0.07$), while the biggest improvement (average increase of $F = 0.13$) in autumn was in high illumination areas. Broadleaf forest accuracy using corrected imagery improved mostly in low illumination areas both for summer (average increase of $F = 0.16$) and autumn (average increase of $F = 0.1$). However, mixed forest had the highest classification improvement in high illumination areas for both summer (average increase of $F = 0.06$) and autumn (average increase of $F = 0.32$) images.

4. Discussion

Monitoring forests in mountains is of great importance to understand ecological and societal processes, yet difficult to do with remote sensing because of topographic effects. However, there are now several approaches available that integrate topographic correction with atmospheric correction. We tested two integrated topographic correction approaches and evaluated forest cover classifications based on topographically uncorrected and corrected imagery acquired in summer and autumn, and DOY composite and spectral-temporal metrics derived from a full Landsat time series. We found that the effects of topography on classification accuracy varied among forest types, seasons, and locations but that topographic correction resulted in consistent forest maps. The physical model approach to correct imagery clearly generated the best classification results no matter which inputs were used for classification. Including terrain information can reduce classification error, yet it cannot replace topographic correction, and nor can a full time series and spectral-temporal metrics.

Both our enhanced C-correction method and the physical model improved our forest classifications. The choice of topographic correction method is vital for a success of forest classification. However, some correction approaches such as the cosine correction underestimate the reflectance of sun-facing slopes and overestimates the reflectance of slopes facing away from the sun (Gu and Gillespie, 1998). This under- and over-correction introduce errors that offset the benefits of topographic correction. Because of the lack of reference for an independent evaluation, existing studies often use indirect measurements such as visual analysis or correlation analysis to evaluate model performance (Sola et al., 2016). Here we assessed the performance of our enhanced C-correction and the physical model by examining (1) the relationship between the illumination condition and the spectral reflectance and (2) forest classification accuracy before and after topographic correction. Our results suggested that both types of corrections reduced the relationship between spectral reflectance and illumination condition (Fig. 4), which resulted in a better separability of multiple land cover classes (Fig. 5A). We suggest that this is the reason why we achieved

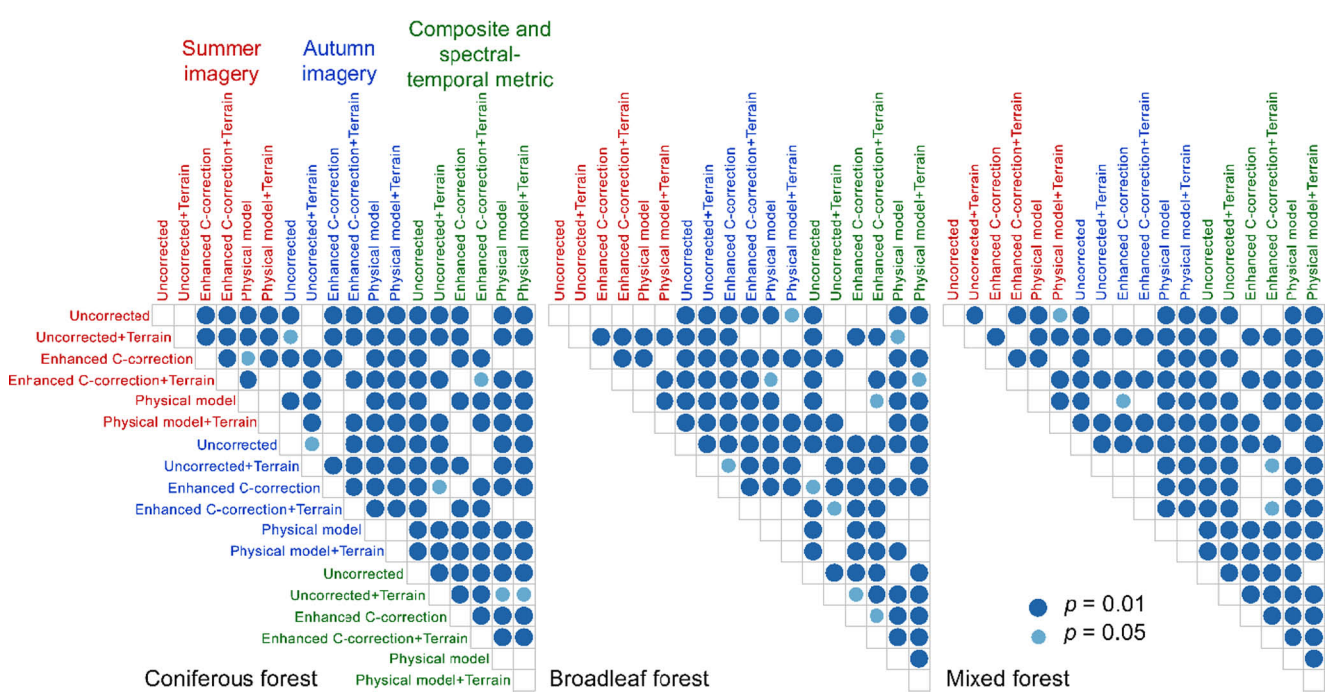

Fig. 8. The significance level (p) of McNemar's test of pair-wise classification comparison for coniferous, broadleaf and mixed forest.

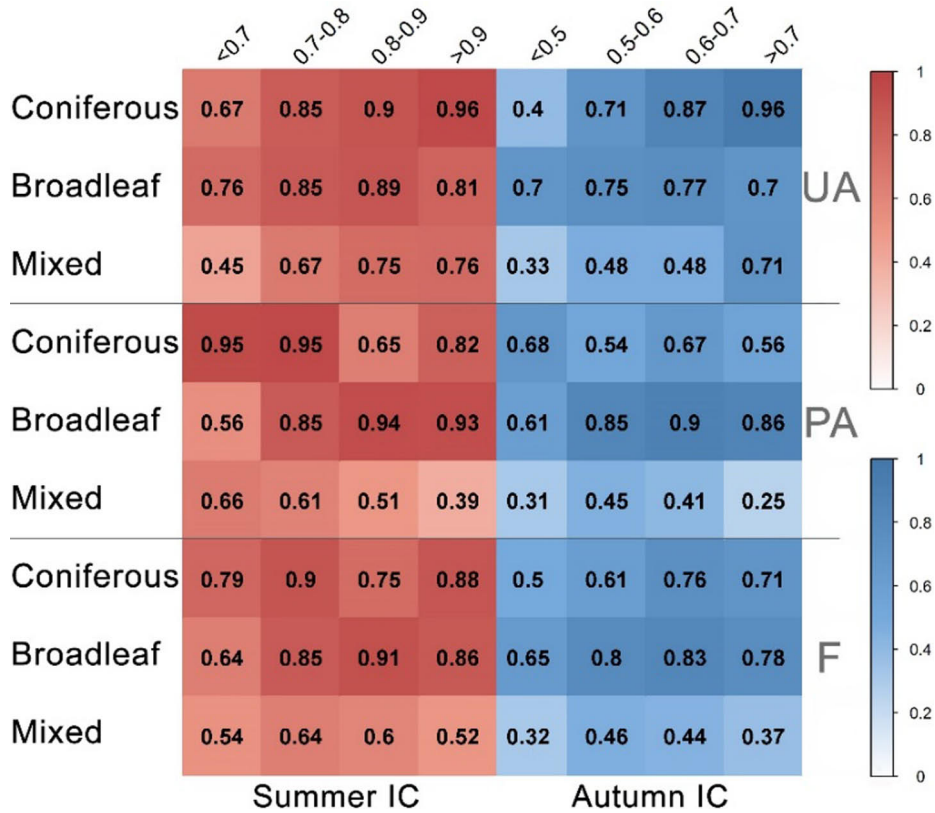

Fig. 9. User's accuracy (UA), producer's accuracy (PA), and F-measure (F) of coniferous, broadleaf and mixed forests among different illumination condition (IC) intervals for classifications using uncorrected summer (red color) and autumn imagery (blue color).

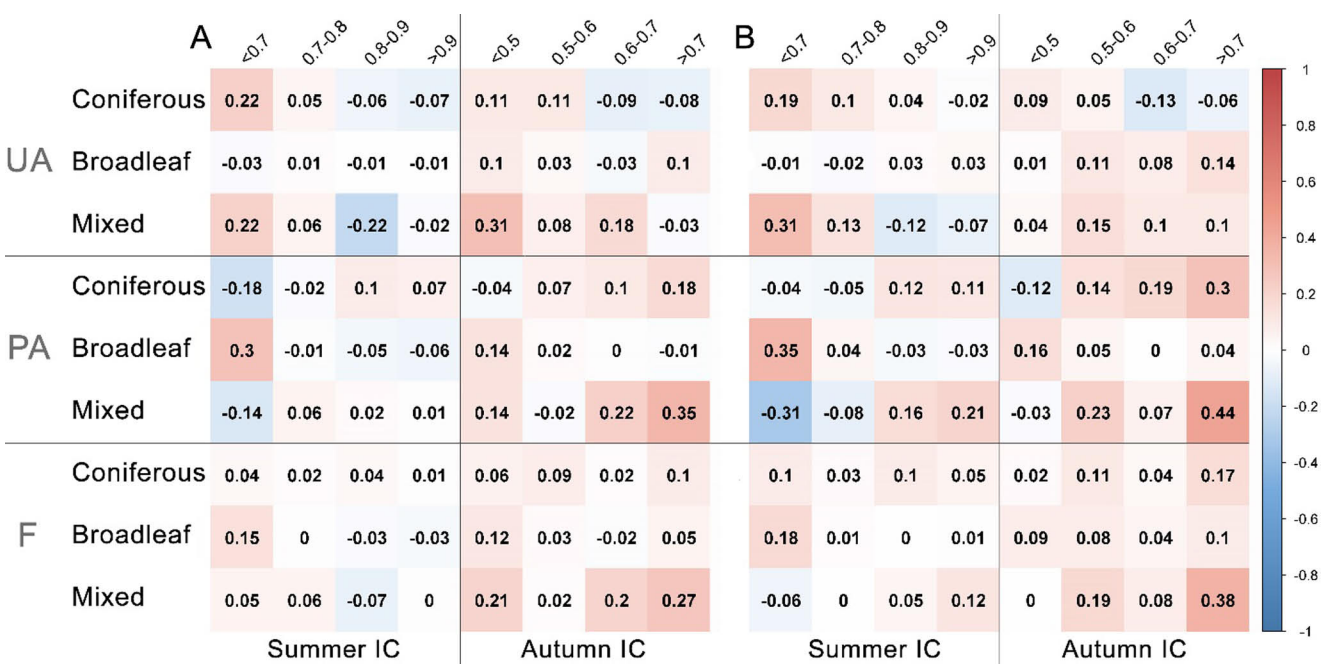

Fig. 10. Differences in user's accuracy (UA), producer's accuracy (PA) and F-measure (F) between classifications using enhanced C-correction (A), physical model (B), and uncorrected imagery of coniferous, broadleaf and mixed forests for different intervals of illumination conditions (IC). Red colors indicate improved mapping accuracy using corrected imagery while blues indicate decreased accuracy.

higher forest mapping accuracy using the topographically corrected imagery (Fig. 7).

The physical model used in this study does not require the empirical parameters derived from the imagery and thus is scene independent. This has important implications for forest cover classification and change detection using multi-temporal and multi-sensor imagery (e.g., Sentinel-2) because the physical model can generate radiometrically homogeneous imagery. On the other hand, the inclusion of a per-pixel C-

factor, which is coupled to atmospheric conditions, has the advantage of more locally describing surface anisotropy, which is assumed to be strictly Lambertian in the physical model. However, in our tests, the enhanced C-correction performed not as well as the physical model. This may be due to several reasons: (1) the atmospheric modelling in the enhanced C-correction used a modified 5S code, which may have modelled the diffuse and direct components of the illumination less precisely than the 6S code used in the physical model; (2) different implementations of atmospheric correction and image-based aerosol retrieval may have resulted in different estimates of atmospheric aerosol content, which in turn affecting the separation of direct and diffuse light, as well as on the propagation of C through the spectrum; (3) the enhanced C-correction only employed a simplified sky view factor as opposed to the more elaborate - but computationally expensive - ray tracing approach used for the physical model. Nevertheless, we recommend FORCE for topographic correction because of its capacity and availability. In addition, a newer version of FORCE v3.6.3 was released recently and we found mapping accuracy can be further improved (Fig. 6A).

We found that the effects of topographic correction varied among forest types, seasons and locations yet the topographic correction generated consistent forest maps. Chance et al. (2016) showed that topographic correction may not be needed in forest change detection using the best-available-pixel composites derived from July and August imagery. We found that the broadleaf forest classification using corrected summer imagery had no significant improvement (McNemar's test $p > 0.05$) but coniferous and mixed forest mapping accuracies improved significantly (McNemar's test $p \leq 0.05$). The insignificant improvement in broadleaf forest classification might be due to the high classification accuracy of broadleaf forest in flat areas such as the Colchis Lowlands (Fig. 1). However, accuracy differences among different illumination conditions showed obvious improvement in broadleaf forest classification in rugged terrain (Fig. 10). Vanonckelen et al. (2013) found that topographic correction had the biggest effects in low-illuminated slopes. We found that the correction was beneficial in both low and high illuminated areas, depending on the date of imagery. The effect of topographic correction was most obvious in the low-illuminated areas in summer imagery while the improvement was highest in high illuminated areas in autumn imagery. One reason could be that the random forest classifier tends to predict the dominant classes (Pal, 2005). In summer, most of the forested area had high illuminations while in autumn most forested area had low-illumination conditions. Thus, forests in the low-illuminated areas tended to be misclassified in summer while in autumn they were classified correctly. Because topographic correction normalized feature variations due to illumination it consistently resulted in accurate forest maps (Fig. 6). Overall, our approach clearly demonstrated the need of topographic correction for satellite imagery from any season when conducting classifications.

Topographic correction contributed most to the classification accuracy of complex forest types. As an ecological hot spot, our study area encompasses diverse tree species ranging from sub-tropical trees to temperate conifers. The overlap of spectral signatures and the confounding topographic effects make it difficult to map heterogeneous forests, and the mixed forest class had the lowest classification accuracy. Using topographic corrected imagery resulted in the greatest accuracy improvement for the mixed forest class (Fig. 7) mostly because the within-class variance in reflectance was reduced. This highlights the value of topographic correction in a heterogeneous environment. We found only slight accuracy improvements (e.g., <5%) for the herbaceous land, water, and un-vegetated classes using corrected imagery for classification (Figs. 7-11A). This is not surprising because these three classes had already high mapping accuracies before the topographic correction was applied. More importantly, herbaceous land and water were less affected by the topographic effects compared to the forests because forests were more distributed on the slopes. This is the reason why we mainly focused on forest mapping.

Topographic correction is necessary when analyzing a full time series of satellite data. The F-measures increased significantly using the topographically corrected DOY composite and spectral-temporal metrics, especially for the mixed forest classification (Figs. 7, 8). Our findings have broader implications for large scale mapping initiatives because the DOY composite and spectral-temporal metrics from Landsat- imagery are often used for large area gap-free mapping (Gómez et al., 2016). Furthermore, with the release of topographic correction tools (e.g., FORCE), it is possible to correct all available Landsat imagery in an operational way. Including the terrain information in the classification reduced classification error but could not replace topographic correction. Similar to findings in previous studies (Elumnoh and Shrestha, 2000; Zhu et al., 2016), our results confirmed that terrain information such as the topographic slope, elevation, and aspect improved forest classification accuracy in mountains. Yet, topographic effects cannot be eliminated by only using the terrain data. This is partly because the topographic effects change over time, yet the terrain data are static. However, we recommend including terrain data in the classification model because auxiliary information depicting the abiotic factors that affect vegetation distribution can improve to distinguish land cover classes.

Further considerations to improve the utility of topographic correction for forest classification in mountains include, first, better quality and higher resolution DEM data for topographic correction. To calculate topographic slope and aspect for one pixel from the SRTM DEM, the neighboring pixels have to be included, which de facto decreases the spatial resolution to 90 m. Though there is no conclusive suggestion regarding the optimal resolution of DEM for correction, most studies suggested that the resolution of the DEM used for topographic correction should be smaller than the resolution of the satellite images (Conese et al., 1993; Hantson and Chuvieco, 2011). In addition, the co-registration errors between DEM and Landsat images may be another error source. A better co-registered DEM may further improve the performance of topographic correction. Second, while self-shadow shaded areas are relatively easy to identify, it is more difficult to identify areas affected by cast shadows because the assumption that the observed radiance is a function of illumination condition angle is violated (Li et al., 2012). Furthermore, Landsat 7 and older imagery has a limited radiometric resolution, making it difficult to estimate reflectance in dark area. However, the better radiometric resolution of Landsat 8 and Sentinel-2 might make it feasible to correct cast shadow areas. Third, our results were based on Landsat imagery, which may suggest the value of topographic correction for forest mapping when using other Landsat-like imagery. To this end, our methods can also be transferred to the imagery from other sensors such as Sentinel-2 (e.g., Grabska et al., 2020). Last, in this study we focused on the topographic effect only and did not take adjacency effect and bi-directional reflectance distribution function (BRDF) into account. The mapping accuracy might be further improved if such corrections were also included.

While we focused our forest classification on the Caucasus region, our findings are probably also applicable for classifying forests elsewhere where the illumination conditions are similar, such as other temperate regions with high topographic relief. Further tests especially in the tropics and subarctic regions are necessary though to understand how topographic correction can perform at a global scale. Other studies, however, suggest a positive effect of topographic correction on land cover classification in the high latitudes and tropics (Adhikari et al., 2016; Heiskanen et al., 2002). In summary, with the increasing availability of topographic correction approaches, we recommend using topographic corrected imagery for forest cover classification especially in mountainous regions.

Declaration of Competing Interest

The authors declare that they have no known competing financial interests or personal relationships that could have appeared to influence

the work reported in this paper.

Acknowledgements

We gratefully acknowledge support for this research by the Land-Cover and Land-Use Change (LCLUC) Program of the National Aeronautic and Space Administration (NASA) through grants NNX15AD93G and 80NSSC18K0316. We thank J. Buchner and K. Lewińska for their constructive suggestions to the manuscript.

Appendix A. Supplementary material

Supplementary data to this article can be found online at https://doi.org/10.1016/j.jag.2022.102716.

References

Adhikari, H., Heiskanen, J., Maeda, E.E., Pellikka, P.K.E., 2016. The effect of topographic normalization on fractional tree cover mapping in tropical mountains: An assessment based on seasonal Landsat time series. Int. J. Appl. Earth Obs. Geoinf. 52, 20–31. https://doi.org/10.1016/J.JAG.2016.05.008.

Agrest, A., 1990. Categorical data analysis. Wiley, New York.

Balthazar, V., Vanacker, V., Lambin, E.F., 2012. Evaluation and parameterization of ATCOR3 topographic correction method for forest cover mapping in mountain areas. Int. J. Appl. Earth Obs. Geoinf. 18, 436–450. https://doi.org/10.1016/j.jag.2012.03.010.

Banskota, A., Kayastha, N., Falkowski, M.J., Wulder, M.A., Froese, R.E., White, J.C., 2014. Forest Monitoring Using Landsat Time Series Data: A Review. Can. J. Remote Sens. 40 (5), 362–384. https://doi.org/10.1080/07038992.2014.987376.

Belgiu, M., Drăguţ, L., 2016. Random forest in remote sensing: A review of applications and future directions. ISPRS J. Photogramm. Remote Sens. 114, 24–31. https://doi.org/10.1016/J.ISPRSJPRS.2016.01.011.

Blesius, L., Weirich, F., 2005. The use of the Minnaert correction for land-cover classification in mountainous terrain. Int. J. Remote Sens. 26 (17), 3831–3851. https://doi.org/10.1080/01431160500104194.

Bragina, E.V., Radeloff, V.C., Baumann, M., Wendland, K., Kuemmerle, T., Pidgeon, A.M., 2015. Effectiveness of protected areas in the Western Caucasus before and after the transition to post-socialism. Biol. Conserv. 184, 456–464. https://doi.org/10.1016/j.biocon.2015.02.013.

Buchner, J., Yin, H.e., Frantz, D., Kuemmerle, T., Askerov, E., Bakuradze, T., Bleyhl, B., Elizbarashvili, N., Komarova, A., Lewińska, K.E., Rizayeva, A., Sayadyan, H., Tan, B., Tepanosyan, G., Zazanashvili, N., Radeloff, V.C., 2020. Land-cover change in the Caucasus Mountains since 1987 based on the topographic correction of multi-temporal Landsat composites. Remote Sens. Environ. 248, 111967. https://doi.org/10.1016/j.rse.2020.111967.

Chance, C.M., Hermosilla, T., Coops, N.C., Wulder, M.A., White, J.C., 2016. Effect of topographic correction on forest change detection using spectral trend analysis of Landsat pixel-based composites. Int. J. Appl. Earth Obs. Geoinf. 44, 186–194. https://doi.org/10.1016/j.jag.2015.09.003.

Civco, D.L., 1989. Topographic normalization of Landsat Thematic Mapper digital imagery. Photogramm. Eng. Remote Sensing 55, 1303–1309.

Conese, C., Gilabert, M.A., Maselli, F., Bottai, L., 1993. Topographic normalization of TM scenes through the use of an atmospheric correction method and digital terrain model. Photogramm. Eng. Remote Sensing 59, 1745–1753.

DomaÇ, A., Süzen, M.L., 2006. Integration of environmental variables with satellite images in regional scale vegetation classification. Int. J. Remote Sens. 27 (7), 1329–1350. https://doi.org/10.1080/01431160500444806.

Dorren, L.K.A., Maier, B., Seijmonsbergen, A.C., 2003. Improved Landsat-based forest mapping in steep mountainous terrain using object-based classification. For. Ecol. Manage. 183 (1-3), 31–46. https://doi.org/10.1016/S0378-1127(03)00113-0.

Doxani, G., Vermote, E., Roger, J.-C., Gascon, F., Adriaensen, S., Frantz, D., Hagolle, O., Hollstein, A., Kirches, G., Li, F., Louis, J., Mangin, A., Pahlevan, N., Pflug, B., Vanhellemont, Q., Doxani, G., Vermote, E., Roger, J.-C., Gascon, F., Adriaensen, S., Frantz, D., Hagolle, O., Hollstein, A., Kirches, G., Li, F., Louis, J., Mangin, A., Pahlevan, N., Pflug, B., Vanhellemont, Q., 2018. Atmospheric correction inter-comparison exercise. Remote Sens. 10, 352. https://doi.org/10.3390/rs10020352.

Dwyer, J., Roy, D., Sauer, B., Jenkerson, C., Zhang, H., Lymburner, L., Dwyer, J.L., Roy, D.P., Sauer, B., Jenkerson, C.B., Zhang, H.K., Lymburner, L., 2018. Analysis Ready Data: Enabling analysis of the Landsat archive. Remote Sens. 2018, Vol. 10, Page 1363 10, 1363. https://doi.org/10.3390/RS10091363.

Ekstrand, S., 1996. Landsat TM-Based Forest Damage Assessment: Correction for Topographic Effects. Photogramm. Eng. Remote Sens. 62, 151–161.

Elumnoh, A., Shrestha, R.P., 2000. Application of DEM data to Landsat image classification: Evaluation in a tropical wet-dry landscape of Thailand. Photogramm. Eng, Remote Sens.

Farr, T.G., Rosen, P.A., Caro, E., Crippen, R., Duren, R., Hensley, S., Kobrick, M., Paller, M., Rodriguez, E., Roth, L., Seal, D., Shaffer, S., Shimada, J., Umland, J., Werner, M., Oskin, M., Burbank, D., Alsdorf, D.E., 2007. The Shuttle Radar Topography Mission. Rev. Geophys. 45, 2004. https://doi.org/10.1029/2005RG000183.

Frantz, D., 2019. FORCE—Landsat + Sentinel-2 Analysis Ready Data and Beyond. Remote Sens. 11, 1124. https://doi.org/10.3390/rs11091124.

Frantz, D., Roder, A., Stellmes, M., Hill, J., 2016. An Operational Radiometric Landsat Preprocessing Framework for Large-Area Time Series Applications. IEEE Trans. Geosci. Remote Sens. 54 (7), 3928–3943. https://doi.org/10.1109/TGRS.2016.2530856.

Frantz, D., Stellmes, M., 2018. Water vapor database for atmospheric correction of Landsat imagery. PANGAEA.

Gao, B., 2015. MODIS Atmosphere L2 Water Vapor Product. NASA MODIS Adaptive Processing System, Goddard Space Flight Center, USA: https://doi.org/10.5067/MODIS/MOD05_L2.006.

Gómez, C., White, J.C., Wulder, M.A., 2016. Optical remotely sensed time series data for land cover classification: A review. ISPRS J. Photogramm. Remote Sens. 116, 55–72. https://doi.org/10.1016/J.ISPRSJPRS.2016.03.008.

Grabska, E., Frantz, D., Ostapowicz, K., 2020. Evaluation of machine learning algorithms for forest stand species mapping using Sentinel-2 imagery and environmental data in the Polish Carpathians. Remote Sens. Environ. 251, 112103.

Griffiths, P., van der Linden, S., Kuemmerle, T., Hostert, P., 2013. A pixel-based Landsat compositing algorithm for large area land cover mapping. IEEE J. Sel. Top. Appl. Earth Obs. Remote Sens. 6 (5), 2088–2101. https://doi.org/10.1109/JSTARS.2012.2228167.

Gu, D., Gillespie, A., 1998. Topographic Normalization of Landsat TM Images of Forest Based on Subpixel Sun–Canopy–Sensor Geometry. Remote Sens. Environ. 64 (2), 166–175. https://doi.org/10.1016/S0034-4257(97)00177-6.

Hannah, L., Carr, J.L., Lankerani, A., 1995. Human disturbance and natural habitat: a biome level analysis of a global data set. Biodivers. Conserv. 4 (2), 128–155. https://doi.org/10.1007/BF00137781.

Hansen, M.C., Egorov, A., Potapov, P.V., Stehman, S.V., Tyukavina, A., Turubanova, S.A., Roy, D.P., Goetz, S.J., Loveland, T.R., Ju, J., Kommareddy, A., Kovalskyy, V., Forsyth, C., Bents, T., 2014. Monitoring conterminous United States (CONUS) land cover change with Web-Enabled Landsat Data (WELD). Remote Sens. Environ. 140, 466–484. https://doi.org/10.1016/j.rse.2013.08.014.

Hansen, M.C., Potapov, P.V., Moore, R., Hancher, M., Turubanova, S.A., Tyukavina, A., Thau, D., Stehman, S.V., Goetz, S.J., Loveland, T.R., Kommareddy, A., Egorov, A., Chini, L., Justice, C.O., Townshend, J.R.G., 2013. High-Resolution Global Maps of 21st-Century Forest Cover Change. Science 342 (6160), 850–853.

Hantson, S., Chuvieco, E., 2011. Evaluation of different topographic correction methods for Landsat imagery. Int. J. Appl. Earth Obs. Geoinf. 13 (5), 691–700. https://doi.org/10.1016/j.jag.2011.05.001.

Heiskanen, J., Kajuutti, K., Jackson, M., Elvehøy, H., Pellikka, P., 2002. Assessment of glaciological parameters using Landsat satellite data in Svartisen, northern Norway, in: Proceedings of EARSeL-LISSIG-Workshop Observing Our Cryosphere from Space. Bern.

Hill, J., Mehl, W., Radeloff, V.C., 1995. Improved forest mapping by combining corrections of atmospheric and topographic effects in Landsat TM imagery, in: Askne (Ed.), Sensors and Environmental Applications of Remote Sensing. Balkena, Rotterdam.

Huang, H., Gong, P., Clinton, N., Hui, F., 2008. Reduction of atmospheric and topographic effect on Landsat TM data for forest classification. Int. J. Remote Sens. 29 (19), 5623–5642. https://doi.org/10.1080/01431160802082148.

Hurni, K., Van Den Hoek, J., Fox, J., 2019. Assessing the spatial, spectral, and temporal consistency of topographically corrected Landsat time series composites across the mountainous forests of Nepal. Remote Sens. Environ. 231, 111225. https://doi.org/10.1016/j.rse.2019.111225.

Kobayashi, S., Sanga-Ngoie, K., 2008. The integrated radiometric correction of optical remote sensing imageries. Int. J. Remote Sens. 29 (20), 5957–5985. https://doi.org/10.1080/01431160701881889.

Koetz, B., Morsdorf, F., van der Linden, S., Curt, T., Allgöwer, B., 2008. Multi-source land cover classification for forest fire management based on imaging spectrometry and LiDAR data. For. Ecol. Manage. 256 (3), 263–271. https://doi.org/10.1016/j.foreco.2008.04.025.

Langner, A., Miettinen, J., Siegert, F., 2007. Land cover change 2002–2005 in Borneo and the role of fire derived from MODIS imagery. Global Change Biol 13 (11), 2329–2340.

Li, A., Wang, Q., Bian, J., Lei, G., 2015. An Improved Physics-Based Model for Topographic Correction of Landsat TM Images. Remote Sens. 7, 6296–6319. https://doi.org/10.3390/rs70506296.

Li, F., Jupp, D.L.B., Thankappan, M., Lymburner, L., Mueller, N., Lewis, A., Held, A., 2012. A physics-based atmospheric and BRDF correction for Landsat data over mountainous terrain. Remote Sens. Environ. 124, 756–770. https://doi.org/10.1016/J.RSE.2012.06.018.

Liang, S., 2005. Topographic correction methods. In: Quantitative Remote Sensing of Land Surfaces. John Wiley & Sons Inc, Hoboken, NJ, USA, pp. 231–244. https://doi.org/10.1002/047172372X.ch3.

Liu, Y., Gong, W., Hu, X., Gong, J., 2018. Forest type identification with random forest using Sentinel-1A, Sentinel-2A, multi-temporal Landsat-8 and DEM data. Remote Sens 10 (6), 946. https://doi.org/10.3390/rs10060946.

Martinuzzi, S., Gould, W.A., Ramos González, O.M., 2007. Land development, land use, and urban sprawl in Puerto Rico integrating remote sensing and population census data. Landsc. Urban Plan. 79 (3-4), 288–297. https://doi.org/10.1016/j.landurbplan.2006.02.014.

Meyer, P., Itten, K.I., Kellenberger, T., Sandmeier, S., Sandmeier, R., 1993. Radiometric corrections of topographically induced effects on Landsat TM data in an alpine environment. ISPRS J. Photogramm. Remote Sens. 48 (4), 17–28. https://doi.org/10.1016/0924-2716(93)90028-L.

Mikkola, J., Pellikka, P., 2002. Normalization of bi-directional effects in aerial CIR photographs to improve classification accuracy of boreal and subarctic vegetation for pollen-landscape calibration. Int. J. Remote Sens. 23 (21), 4719–4742. https://doi.org/10.1080/01431160110113944.

Minnaert, M., 1941. The reciprocity principle in lunar photometry. Astrophys. J. 93, 403. https://doi.org/10.1086/144279.

Moreira, E.P., Valeriano, M.M., 2014. Application and evaluation of topographic correction methods to improve land cover mapping using object-based classification. Int. J. Appl. Earth Obs. Geoinf. 32, 208–217. https://doi.org/10.1016/J.JAG.2014.04.006.

Pal, M., 2005. Random forest classifier for remote sensing classification. Int. J. Remote Sens. 26 (1), 217–222. https://doi.org/10.1080/01431160412331269698.

Pauleit, S., Duhme, F., 2000. Assessing the environmental performance of land cover types for urban planning. Landsc. Urban Plan. 52 (1), 1–20. https://doi.org/10.1016/S0169-2046(00)00109-2.

Pellikka, P., 1996. Illumination compensation for aerial video images to increase land cover classification accuracy in mountains. Can. J. Remote Sens. 22 (4), 368–381. https://doi.org/10.1080/07038992.1996.10874661.

Phiri, D., Morgenroth, J., Xu, C., Hermosilla, T., 2018. Effects of pre-processing methods on Landsat OLI-8 land cover classification using OBIA and random forests classifier. Int. J. Appl. Earth Obs. Geoinf. 73, 170–178. https://doi.org/10.1016/j.jag.2018.06.014.

Pielke, R.A., 2005. Land use and climate change. Science 310 (5754), 1625–1626.

Pimple, U., Sitthi, A., Simonetti, D., Pungkul, S., Leadprathom, K., Chidthaisong, A., 2017. Topographic Correction of Landsat TM-5 and Landsat OLI-8 Imagery to Improve the Performance of Forest Classification in the Mountainous Terrain of Northeast Thailand. Sustainability 9, 258. https://doi.org/10.3390/su9020258.

Pitman, A.J., de Noblet-Ducoudré, N., Cruz, F.T., Davin, E.L., Bonan, G.B., Brovkin, V., Claussen, M., Delire, C., Ganzeveld, L., Gayler, V., van den Hurk, B.J.J.M., Lawrence, P.J., van der Molen, M.K., Müller, C., Reick, C.H., Seneviratne, S.I., Strengers, B.J., Voldoire, A., 2009. Uncertainties in climate responses to past land cover change: First results from the LUCID intercomparison study. Geophys. Res. Lett. 36 (14) https://doi.org/10.1029/2009GL039076.

Powers, D.M.W., 2011. Evaluation: From precision, recall and f-measure to roc, informedness, markedness and correlation. J. Mach. Learn. Technol. 2, 37–63.

Richter, R., 1998. Correction of satellite imagery over mountainous terrain. Appl. Opt. 37 (18), 4004. https://doi.org/10.1364/AO.37.004004.

Richter, R., 1996. Atmospheric correction of satellite data with haze removal including a haze/clear transition region. Comput. Geosci. 22 (6), 675–681. https://doi.org/10.1016/0098-3004(96)00010-6.

Richter, R., Kellenberger, T., Kaufmann, H., 2009. Comparison of topographic correction methods. Remote Sens. 1, 184–196. https://doi.org/10.3390/rs1030184.

Sanderson, E.W., Jaiteh, M., Levy, M.A., Redford, K.H., Wannebo, A.V., Woolmer, G., 2002. The Human Footprint and the Last of the Wild. Bioscience 52, 891. https://doi.org/10.1641/0006-3568(2002)052[0891:THFATL]2.0.CO;2.

Santini, F., Palombo, A., 2019. Physically Based Approach for Combined Atmospheric and Topographic Corrections. Remote Sens. 11, 1218. https://doi.org/10.3390/rs11101218.

Sola, I., González-Audícana, M., Álvarez-Mozos, J., 2016. Multi-criteria evaluation of topographic correction methods. Remote Sens. Environ. 184, 247–262. https://doi.org/10.1016/j.rse.2016.07.002.

Tan, B., Masek, J.G., Wolfe, R., Gao, F., Huang, C., Vermote, E.F., Sexton, J.O., Ederer, G., 2013. Improved forest change detection with terrain illumination corrected Landsat images. Remote Sens. Environ. 136, 469–483. https://doi.org/10.1016/j.rse.2013.05.013.

Tanre, D., Herman, M., Deschamps, P.Y., de Leffe, A., 1979. Atmospheric modeling for space measurements of ground reflectances, including bidirectional properties. Appl. Opt. 18 (21), 3587. https://doi.org/10.1364/AO.18.003587.

Teillet, P.M., Guindon, B., Goodenough, D.G., 1982. On the slope-aspect correction of multispectral scanner data. Can. J. Remote Sens. 8 (2), 84–106. https://doi.org/10.1080/07038992.1982.10855028.

Vanonckelen, S., Lhermitte, S., Balthazar, V., Van Rompaey, A., 2014. Performance of atmospheric and topographic correction methods on Landsat imagery in mountain areas. Int. J. Remote Sens. 35 (13), 4952–4972. https://doi.org/10.1080/01431161.2014.933280.

Vanonckelen, S., Lhermitte, S., Van Rompaey, A., 2013. The effect of atmospheric and topographic correction methods on land cover classification accuracy. Int. J. Appl. Earth Obs. Geoinf. 24, 9–21. https://doi.org/10.1016/j.jag.2013.02.003.

Vermote, E.F., El Saleous, N., Justice, C.O., Kaufman, Y.J., Privette, J.L., Remer, L., Roger, J.C., Tanré, D., 1997. Atmospheric correction of visible to middle-infrared EOS-MODIS data over land surfaces: Background, operational algorithm and validation. J. Geophys. Res. 102 (D14), 17131–17141.

Vicente-Serrano, S., Perez-Cabello, F., Lasanta, T., 2008. Assessment of radiometric correction techniques in analyzing vegetation variability and change using time series of Landsat images. Remote Sens. Environ. 112 (10), 3916–3934. https://doi.org/10.1016/j.rse.2008.06.011.

White, J.C., Wulder, M.A., Hobart, G.W., Luther, J.E., Hermosilla, T., Griffiths, P., Coops, N.C., Hall, R.J., Hostert, P., Dyk, A., Guindon, L., 2014. Pixel-based image compositing for large-area dense time series applications and science. Can. J. Remote Sens. 40 (3), 192–212. https://doi.org/10.1080/07038992.2014.945827.

Woodcock, C.E., Allen, R., Anderson, M., Belward, A., Bindschadler, R., Cohen, W., Gao, F., Goward, S.N., Helder, D., Helmer, E., Nemani, R., Oreopoulos, L., Schott, J., Thenkabail, P.S., Vermote, E.F., Vogelmann, J., Wulder, M.A., Wynne, R., 2008. Free access to Landsat imagery. Science (80-. 320 (5879), 1011.

Wulder, M.A., Coops, N.C., Roy, D.P., White, J.C., Hermosilla, T., 2018. Land cover 2.0. Int. J. Remote Sens. 39 (12), 4254–4284. https://doi.org/10.1080/01431161.2018.1452075.

Wulder, M.A., White, J.C., Loveland, T.R., Woodcock, C.E., Belward, A.S., Cohen, W.B., Fosnight, E.A., Shaw, J., Masek, J.G., Roy, D.P., 2016. The global Landsat archive: Status, consolidation, and direction. Remote Sens. Environ. 185, 271–283.

Yin, H.e., Brandão, A., Buchner, J., Helmers, D., Iuliano, B.G., Kimambo, N.E., Lewińska, K.E., Razenkova, E., Rizayeva, A., Rogova, N., Spawn, S.A., Xie, Y., Radeloff, V.C., 2020. Monitoring cropland abandonment with Landsat time series. Remote Sens. Environ. 246, 111873. https://doi.org/10.1016/j.rse.2020.111873.

Yin, H., Khamzina, A., Pflugmacher, D., Martius, C., 2017. Forest cover mapping in post-Soviet Central Asia using multi-resolution remote sensing imagery. Sci. Rep. 7, 1375.

Zazanashvili, N., Gagnidze, R., Nakhutsrishvili, G., 2000. Main types of vegetation zonation on the mountains of the Caucasus. Acta Phytogeogr. Suec. 85, 7–16.

Zhu, Z., Gallant, A.L., Woodcock, C.E., Pengra, B., Olofsson, P., Loveland, T.R., Jin, S., Dahal, D., Yang, L., Auch, R.F., 2016. Optimizing selection of training and auxiliary data for operational land cover classification for the LCMAP initiative. ISPRS J. Photogramm. Remote Sens. 122, 206–221. https://doi.org/10.1016/J.ISPRSJPRS.2016.11.004.